View metadata, citation and similar papers at core.ac.uk
brought to you by CORE
provided by Electronic Sumy State University Institutional...

FORMATION OF SILICON-BASED NANOSTRUCTURES BY COMPRESSION PLASMA FLOWS

Yury A. Petukhou[1,*], Vladimir V. Uglov[2], Nicolai T. Kvasov[1], Andrey V. Punko[1], Irina L. Doroshevich[1], Valiantsin M. Astashynski[3], Anton M. Kuzmitski[3]

1 Belarusian State University of Informatics and Radioelectronics, Brouka 6, 220013, Minsk, Belarus
2 Belarusian State University, Nezalezhnasti 4, 220030, Minsk, Belarus
3 B.I. Stepanov Institute of Physics, NAS B, Nezalezhnasti 68, 220070, Minsk, Belarus

ABSTRACT

The use of compression flows (CPF) for the formation of metal and silicide nanostructures for data storage devices, thermoelectric materials and solar cells is presented. The action of CPF with injected metallic powder results in the formation of coatings composed of spherical clusters with complex structure: each submicron cluster (0,1-0,2 μm radius) is formed from a number of nanosized ones (10-25 nm radius). The action of CPF on binary "metal-silicon" systems provides formation of branched silicon dendrites (tip radius ~ 200 nm, primary spacing ~ 1,2 μm); interdendritic space is filled with nanostructured (50-100 nm) "silicide-silicon" and "monosilicide-disilicide" composite due to melting of the surface layer, rapid solidification (~ 10^{-3} m/s) and constitutional overcooling. Mechanisms of formation of nanostructured composites on silicon surface and in thick surface layers is discussed in terms of order parameter evolution and non-equilibrium solidification models.

Key words: nanoclusters, silicides, dendrites, eutectics, compression plasma flows

INTRODUCTION

Application of concentrated energy flows for synthesis and modification of novel nanostructured materials is of a particular interest since their thermal, radiation and mechanical action provides non-equilibrium conditions for the formation of low-dimensional structures on the materials surface and in pre-surface layers [1]. Compression plasma flows (CPF) are special type of concentrated energy beams used for this purpose. CPF are generated by the compression and acceleration of plasma beam by its own azimuthal magnetic field. It provides quasi-stationary energy flow with high concentration of particles (1017 cm^{-3}) and energy density (up to 60 J/cm^2). Pulse duration is much longer than that typical for high-energy plasma pulses and is about 150 μs. Interaction of CPF with target surface results in thermalization of CPF kinetic energy and in the formation of shock-compressed layer with high energy density and com-

* e-mail: spadar_pett@tut.by, tel: (+375)297697058

plex configuration of electric and magnetic fields [2, 3].

Thermal, mechanical and radiation action of CPF pulses results in non-equilibrium structural and phase transformations in surface layers of solids and provides formation of novel structures with controlled physical properties [3-7]. In the present work we use of CPF for synthesis of nanostructures on silicon surface (in the form of nanostructured coatings) and in bulk surface layers.

FORMATION OF NANOSTRUCTURED COATINGS ON SILICON

Main peculiarities of CPF-deposition of coatings are strongly non-equilibrium conditions in plasma medium and significant modification of substrate surface. Deposition of metal coatings was performed by the action of CPF with injected metallic powder on single-crystal silicon wafer. This procedure was carried out on magneto-plasma compressor developed in Institute of Physics (National Academy of Sciences of Belarus). In this setup CPF is generated by pulsed discharge between central and peripheral electrodes in vacuum chamber filled with nitrogen (pressure is 400 Pa). Powder was injected to CPF by electromagnetic lifting and by mechanical spilling synchronized with magneto-plasma compressor [7].

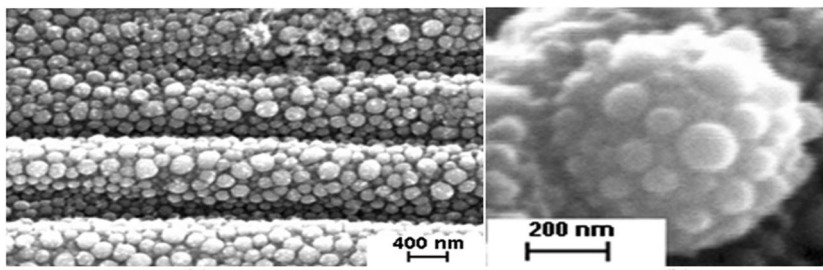

Fig. 1 – SEM-images of iron clusters on CPF-modified silicon

SEM studies revealed the formation of metal layer consisting of spherical clusters with multi-level structure (*Fig.1*). First-level submicron cluster (0,1-0,2 μm radius) is formed from a number of second-level nanosized ones (10-25 nm radius). These clusters are formed in two stages: (1) melting of powder injected to CPF and nucleation of second-level clusters; (2) association of particles in shock-compressed layer, i.e. the formation of first-level clusters [7].

Phase formation in plasma and shock-compressed layer is far from equilibrium and can be described in terms of evolution of order parameter η, taken in the following form:

$$\eta(\omega, \vec{\rho}) = 2\sum_{\vec{q}} \frac{A(\vec{q})\,\Gamma_{\vec{q}}}{(\omega - \omega_{\vec{q}})^2 + \Gamma_{\vec{q}}^2} \cos\left(\vec{q}\cdot\vec{\rho}\right), \quad (1)$$

where $A(\vec{q})$ – amplitude of phase wave with wave vector $\vec{q}$, ρ – cluster radius, $\Gamma_{\vec{q}}$ – damping caused by cluster instability for $\rho < \rho_{\text{cr}}$, ω – phase wave frequency, $\omega_{\vec{q}}$ – characteristic (resonant) frequency of phase wave. Values of $\Gamma_{\vec{q}}$ and $\omega_{\vec{q}}$ for α-th level cluster (α = 0, 1, 2, …) are expressed as

$$\Gamma_{\vec{q}}^{(\alpha+1)} = D_{(\alpha)} q_{(\alpha+1)}^2 + \frac{D_{(\alpha)}}{kT} \int \Delta U_{(\alpha)}(\vec{r}, \vec{r}') n_{(\alpha)}(\vec{r}, t) d^3 r', \tag{2}$$

$$\omega_{\vec{q}}^{(\alpha+1)} = \frac{D_{(\alpha)}}{kT} q_{(\alpha+1)}^2 \int \vec{\nabla} U_{(\alpha)}(\vec{r}, \vec{r}') n_{(\alpha)}(\vec{r}, t) d^3 r',$$

where diffusivity $D_{(\alpha)}$ is found as

$$D_{(\alpha+1)} = D_\alpha \left(\frac{\rho_{(\alpha)}}{\rho_{(\alpha+1)}} \right)^2, \tag{3}$$

where $\rho_{(\alpha)}$ – α-th level cluster radius; $U_{(\alpha)}(\vec{r}, \vec{r}')$ describes potential energy of pair interaction for particles located in points $\vec{r}$ и $\vec{r}'$.

Analysis of first-level cluster formation (Fig.1a) was carried out with the use of Lenard-Jones potential for interaction between atoms and silicon surface:

$$U_{(0)}(\vec{r}, \vec{r}') = A_L \left(B_L |\vec{r} - \vec{r}'|^{-12} - |\vec{r} - \vec{r}'|^{-6} \right). \tag{4}$$

Calculation of Lenard-Jones for iron gives following values: $A_L = 8{,}0 \cdot 10^{-76}$ J·m^6, $B_L = 3{,}2 \cdot 10^{-58}$ m^6.

The formation of second-level clusters from primary ferromagnetic particles (Fig. 1b) was considered as a result of dipole-dipole interaction:

$$U_{(1)}(\vec{r}, \vec{r}') = -\left(\frac{\mu_0}{4\pi} \right)^2 \frac{2 p_1^2 p_2^2}{3kT |\vec{r} - \vec{r}'|^6}, \tag{5}$$

where μ_0 – vacuum permeability , p_1, p_2 – magnetic moments of interacting ferromagnetic particles.

Phase formation starts from cluster with critical radius ρ_{cr} that corresponds to phase wave with vector $\vec{q}_{\text{cr}}$ and characteristic frequency $\omega_{\vec{q}_{\text{cr}}}$. This resonant phenomena results in increase of order parameter $\eta(\omega, \vec{\rho})$. The value of $\vec{q}_{\text{cr}}$ is calculated as:

$$q_{(1)\text{cr}} = \left(\frac{6 \cdot 10^{-74} n^{(0)}(t)}{kT \rho_{(1)\text{cr}}^5} \right)^{1/2}, \tag{6}$$

$$q_{(2)\text{cr}} = \left(\frac{9{,}1 \cdot 10^6 \cdot p_1^2 p_2^2 n^{(1)}(t)}{kT \rho_{(2)\text{cr}}^5} \right)^{1/2}, \tag{7}$$

where $n^{(0)}(t)$ – concentration of primary metal atoms, $n^{(1)}(t)$ – concentration of clusters. Calculations from (6)-(7) performed for iron nanoclusters give values $q_{(1)\mathrm{cr}} = 1{,}04 \cdot 10^9$ m-1, $\nu_q^{(1)\mathrm{cr}} = \frac{\omega_q^{(1)\mathrm{cr}}}{2\pi} = 6 \cdot 10^{13}$ s^{-1}. Thus, stable phase formation occurs in the region with typical radius $\lambda_{\mathrm{cr}} \sim 6 \cdot 10^{-9}$ m. Phase wave velocity for non-equilibrium conditions in plasma and shock-compressed layer is ~3,4·105 m/s.

The formation of nanosized ferromagnetic metal nanostructures makes it possible to develop novel data storage devices based on the arrays of magnetic nanoclusters with high recording density.

COMPRESSION PLASMA FLOWS FOR SILICIDES FORMATION

Metal silicides are widely used in electronics due to their compatibility with silicon technology and wide variety of electrophysical properties subject to element composition, stoichiometry and crystal structure. For example, in Fe-Si binary system α-FeSi2 possesses metallic properties, Fe3Si is a ferromagnetic, FeSi and β-FeSi2 are semiconductors [8-10]. The promising use of silicides in nanotechnology is related with the miniaturization of microelectronic devices and systems to nanoscale, catalysis of nanowire and nanotube growth and others [10-12].

Silicide formation was performed by pre-deposition of metal layer (Fe, Ni, Ti, Zr, Cr, Mo) on silicon wafer followed by CPF treatment with energy density 8-15 J/cm^2 [13]. XRD studies showed the formation of silicides with different stoichiometry in all the treated binary systems (*Fig. 2-3*).

SEM-studies of the samples treated by CPF with power density over 1,0 GW/m2 showed the formation of deep metal-alloyed layer (~ 10 μm thickness) (*Fig. 4*). The use of SEM in elemental contrast mode revealed the formation of silicon dendrites grown throughout the intermixed layer.

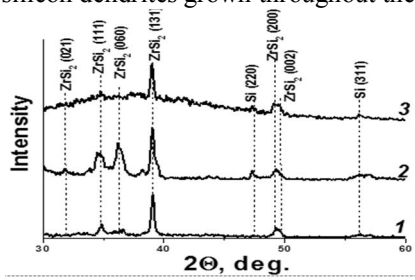

Fig. 2 – XRD patterns of Zr/Si systems treated by CPF with energy density 8 (1), 10 (2) and 14 (3) J/cm^2

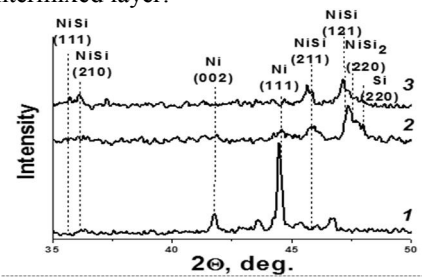

Fig. 3 – XRD patterns of Ni/Si systems treated by CPF with energy density 5 (1), 7 (2) and 13 (3) J/cm^2

Interdendritic space is metal-rich, i.e. metal silicides are preferably localized between silicon dendrites (*Fig. 4-6*). Typical dendrite sizes are following: tip radius 0,2-0,5 μm, primary spacing 0,8-1,5 μm, secondary spacing 0,2-0,9 μm.

Dendrites formation is caused by constitutional overcooling. Low solid-state solubility of metals in silicon lets to metal edging out of solid-liquid interface. According to phase diagrams [14], solidification temperature of metal-rich liquid near the crystallization front is lower than that of silicon, i.e. liquid layer near the solidification interface is overcooled. The evolution of asperities near the crystallization front results in the formation of hexagonal cells and dendrites [15].

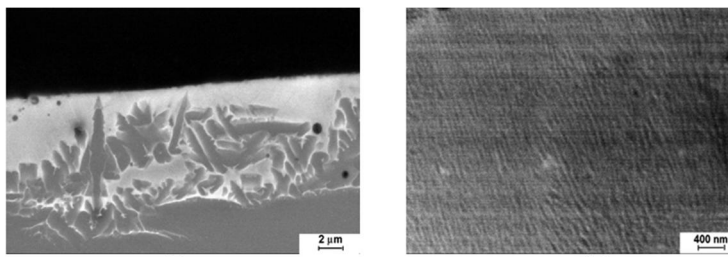

(a) (b)

Fig. 4 – Cross-section SEM-image (10k and 60k magnification) of Mo-Si system treated by CPF with energy density 8 J/cm^2

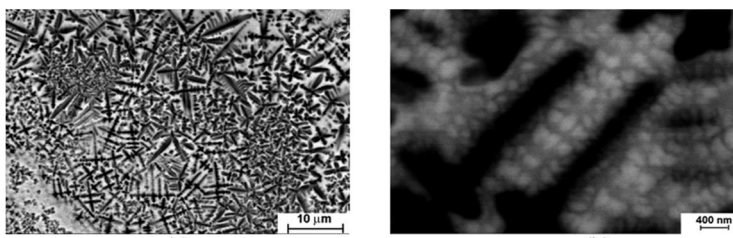

(a) (b)

Fig. 5 – Surface SEM-image (5k and 60k magnification) of Ni-Si system treated by CPF with energy density 13 J/cm^2

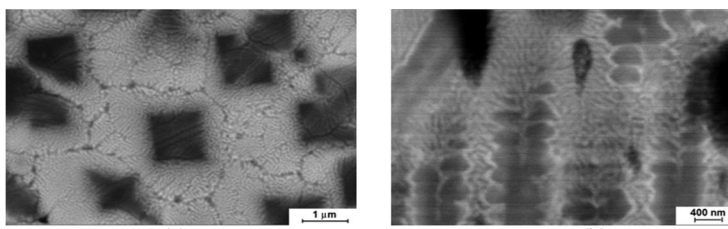

(a) (b)

Fig. 6 – SEM-images of Zr-Si (a) and Ti-Si (b) systems treated by CPF with energy density 12 J/cm^2

SEM studies in elemental contrast mode showed that in CPF-treated Ni-Si system interdendritic space is filled with metal-silicon alloy with globular nickel-rich precipitations 50-200 nm sized and prolonged lamella 0,2-0,6 μm length and lateral size 0,1-0,2 μm. In Ti-Si and Zr-Si systems one observes metal-rich rod and lamellar structure (lateral size 20-50 nm). The formation of these structures is caused by saturation of liquid near the dendritic tip up to eutectic composition. In these conditions liquidus slope changes its sign, so further metal edging decreases constitutional overcooling and dendritic growth slows down. Following self-cooling of inderdendritic liquid results in eutectic solidification.

Since cooling and crystallization occur at velocities ~ 107 K/s. Dendrite formation is properly described by Kurz-Fisher's model [15]. In this model the shape of the cell or dendrite is approximated by ellipsoids and the marginal stability criterion for an isolated dendrite or cell is assumed. This model provides following relationships between geometrical sizes of dendrite and characteristics of solidification process:

$$R = 2\pi\sqrt{\frac{\Gamma D}{m(k-1)C_0 V_d}}, \tag{8}$$

$$\lambda_1 = 4{,}3_4\sqrt{\frac{m(k-1)\Gamma D C_0}{V_d G^2}}, \tag{9}$$

where R – tip radius, $\Gamma = \gamma_{sl}/\Delta S_f$ – Gibbs-Thomson coefficient, γ_{sl} – surface tension coefficient of the melt, ΔS_f –entropy of fusion per volume unit, D – diffusion coefficient in liquid, m – liquidus slope, k – partition coefficient, C_0 – average metal concentration (calculated as ratio of initial iron coating thickness to that of modified layer), V_d – dendritic growth rate, λ_1 – primary dendritic spacing, G – temperature gradient near the solidification front. Calculations in accordance with formulae (8)-(9) (subject to parameters of "metal-silicon" systems [14, 16]) revealed that growth rate estimates 0,04 m/s, and temperature gradient from near the solidification front decreases with the power density of the flow 1,7·108 to 0,8·107 K/m. Temperature gradient decrease is caused by the increase of radiation heat losses at high power densities.

Since eutectic is regular for Zr/Si, Ti/Si and Mo/Si systems and fine grain boundaries are observed (Fig. 6a), silicide and silicon solidify with common isothermal "liquid-solid" interface. In these conditions stability of interface is mainly controlled by constitutional and capillary overcooling. The model developed by Catalina et al. [17] provides relationships between typical sizes of eutectic precipitates and corresponding solidification parameters (overcooling ΔT and interface velocity V_e) for isothermal interface:

$$\lambda = \sqrt{-\frac{1}{V_e}\frac{\mu_r^{Si} - \mu_r^{Me-Si}}{\mu_c^{Si} - \mu_c^{Me-Si}}} \tag{10}$$

where $\mu_r^i = -m_i(1+\xi/(f_i\Omega))(C_E\Omega^2/D)P_i\lambda V$, $\mu_c^i = (2\Gamma_i \sin\theta_i)/(\lambda f_i)$ (superscript i stands for silicide and silicon), $\xi = 1$ for silicide, $\xi = -1$ for silicon, fi – volume fraction of the i-th phase, CE – eutectic concentration, $\Omega = (\rho_{Me-Si}/\rho_L)(1-k_{Me-Si}) - (\rho_{Si}/\rho_L)(1-k_{Si})$, ρ_i and ρ_L are densities of i-th phase and liquid respectively, k_i – segregation coefficient, D – liquid diffusivity, $P_i = \sum_{n=1}^{\infty} \sin^2(n\pi f_i)/(n\pi)^3$, θ_i – contact angle. Calculations performed for silicon and metal silicides showed that formation of eutectic precipitates 60-80 nm size is reached at velocity range 10^{-3}-10^{-4} m/s. The difference between interface velocities for dendritic and eutectic growth is caused by the fact that eutectic solidification start when constitutional overcooling decreases, i.e. dendritic growth slows down.

CONCLUSIONS

The use of CPF with injected metal powder on single-crystal silicon substrate results in the formation of metal coating composed from spherical clusters: each submicron cluster (0,1-0,2 μm radius) is formed from a number of nanosized ones (20-50 nm radius). Nucleation of nanosized clusters is caused by magnetic dipole-dipole interaction between metallic particles, formation of nanocluster layer is provided by condensation of cluster vapor on silicon in shock-compressed plasma layer.

The action of CPF on binary "metal-silicon" systems provides the formation of branched silicon dendrites (tip radius 0,2-0,5 μm, primary spacing 0,8-1,5 μm, secondary spacing 0,2-0,9 μm) with interdendritic space filled with nanostructured (50-100 nm) "silicide-silicon" and "monosilicide-disilicide" composite due to the melting of surface layer followed by rapid eutectic solidification (~10-3 m/s) and constitutional overcooling.

Results of studies show great potential of CPF application for the development of novel nanostructured materials for magnetic, thermoelectric and photovoltaic applications.

Acknoledgements

Authors would like to thank staff scientists Sofia Gusakova, Ludmila Baran and Alexander Kalin (Belarusian State University) for their assistance in SEM-studies and metal deposition procedure.

The work is partially supported by Belarusian Republican Foundation for Fundamental Research (project F10M-127).

REFERENCES

[1] A.D. Pogrebnyak, Yu.N. Tyurin, Physics-Uspekhi, 2005, Vol. 175, No. 5, P. 487-514

[2] A.V. Morozov. Introduction to Plasma Dynamics, Cambridge International Science Publishing, Cambridge, 2010.
[3] V.V. Uglov. V.M. Anishchik, N.N. Cherenda et al., Surface and Coatings Technology, 2005, Vol. 200, P. 297-300.
[4] V.M. Astashynski, S.I. Ananin, E.A. Kostyukevich et al., High Temperature Material Processes, 2007, Vol. 11, №4, P. 537-548.
[5] Method of producing metal silicide: Patent RU 2405228, (V.V. Uglov. N.N. Cherenda, N.T. Kvasov, Ju.A. Petukhov, V.M. Astashinskij, G.Z. Podsobej), Appl. No. 2008149485/28, Publ. 27.11.2010.
[6] V.V. Uglov, N.T. Kvasov, Yu.A. Petukhou et al., 139th TMS Annual Meeting & Exhibition Collected Proceedings, 2010, Seattle, USA, Supplemental Proceedings: Vol. 2: Materials Characterization, Computation, Modeling, Energy, P.633-640.
[7] V.M. Astashynski, V.V. Uglov, N.T. Kvasov et al., VIth International Conference "Plasma Physics and Plasma Technology", 2009, Minsk, Contributed Papers: Vol. I, P.406-409
[8] Semiconducting Silicides (Ed. V.E. Borisenko), Springer-Verlag, Berlin, 2000.
[9] Silicides Technology for Integrated Circuits (Ed. L.J. Chen), The Institution of Engineering and Technology, London, 2009.
[10] S.-F. Chen, H.-C. Chung, C.-P. Liu, Journal of Applied Physics, 2010, Vol 180, 013519 (4 p.)
[11] J.-B. Lee, C.-J. Choi, T.-Y. Seong, Current Applied Physics, 2011, Vol. 11, P. 199-202
[12] J.L. Tedesco, J.E. Rowe, R.J. Nemanich, Journal of Applied Physics, 2010, Vol. 107, 123715 (8 p.)
[13] V. Anishchik, V. Uglov, N. Kvasov et al., Electrical Review, 2010, No. 7, P. 311-313
[14] Smithells Metals Reference Book (Eds. E.A. Brandes, G.B. Brook), Butterworth-Heinemann, Oxford, 1992.
[15] H. Kaya, E. Çadirli, M. Gündüz, Journal of Materials Engineering and Performance, 2006, Vol. 16, No.1, P. 12–21.
[16] K. Tang, E.J. Øvrelid, G. Trannel, M. Tangstad, JOM, 2009, Vol. 61, No.11, P. 49-55.
[17] A.V. Catalina, S. Sen, D.M. Stefanescu, Metal. Mat. Trans., 2003, Vol. 34A, P. 383-394.